Proceedings of the 11th Brazilian Congress of Thermal Sciences and Engineering -- ENCIT 2006
Braz. Soc. of Mechanical Sciences and Engineering -- ABCM, Curitiba, Brazil, Dec. 5-8, 2006

Paper CIT06- 0411

FREEFORM SURFACES MEASUREMENT BY AN OPTICAL SYSTEM OF FRINGE PROJECTION

Sara Del -Vecchio
saradvec@yahoo.com.br

Marcos Pinotti
pinotti@ufmg.br

Meinhard Sesselmann
meinhard@ufmg.br
Mechanical Engineering Department
Federal University of Minas Gerais - UFMG - Antônio Carlos Avenue, 6627, Pampulha, Belo Horizonte – Minas Gerais
CEP: 31270-901

Abstract. An optical system of fringe projection was used to measure a cast iron turbine blade. The system was composed of a LCD projector, a digital photographic camera and a microcomputer. The projection unit illuminated the blade at an oblique angle while the camera observed the specimen under test normally to its central surface point. The blade measurement was obtained through the proccessing of blade images which had shifted fringe patterns projected on its surface. A total of eight images were obtained: four images mutually shifted of ninety degrees for the studied surface and also four for a reference plane. Two types of fringe patterns were tested. Firstly, paralel square grating patterns were adopted and secondly, parallel cosine grating patterns were used. In the last case, different fringe frequencies were also evaluated. The 3D profile was calculated using two dimensional grayscale images by a dedicated software. A brief metrological analysis estimated a uncertainty value of 8%. The main advantages of this system are its easy set up, use of standart optical components, absence of moving parts and its possible applicability at geometric control.

Keywords: Fringe projection, geometrical control, optical system, phase shifting, freeform surfaces.

1. Introduction

The researches on three dimensional (3D) measurement considering optical techniques involve interferometry and also Moiré techniques. Considering Moiré techniques it can be remembered the first studies of Meadows *et al.* (1970) and Takasaki (1970), both developing works of Shadow Moiré, and also Theocaris (1969) and Durelli *et al.* (1970), which made strain evaluation using Projection Moiré, or more widely, Fringe Projection. However, just experimental results were obtained and some problems still remained mainly considering the automatic analysis and determination of fringe orders. Later, with the studies of the phase shifting method of Yoshizawa and Otani (1989) and also the interferometry researches of Post *et al.* (1994), the measurement accuracy of these optical techniques went to the micrometer scale. But there was the difficult of phase identification for different shiftings, which turned these researches restricted to only continuous surfaces. Moreover, it was not possible to determine automatically the fringe orders and so it was also necessary the human intervention to analyse them in order to obtain the depth information about the studied surface as cited by (LU *et al.*, 2002).

GÄSVIK *et al.* (1989) developed an integrated CAD system composed by a fringe projector, a CCD camera and processing *software*, aiming its application on a machine vision 3D inspection. The projection system was composed by a mercury lamp, a pair of lens and a support for the fringe pattern. This projector was put under an angle of 55º from the object while the camera was positioned normally to its surface. A standard object was used as a reference model. Two images were obtained: one for the standard model and other for the object under inspection. The difference of these two images was calculated digitally and it was used for the 3D profile evaluation.

CARBONE *et al.* (2001) developed a methodology for reverse engineering application based on the integration of a 3D vision sensor and a coordinate measuring machine (CMM). The aim was to rebuild CAD models of complex geometry combining an optical sensor (fringe projection) with a mechanical sensor (CMM), and so reducing the human intervention during measuring. For the vision system, they used a LCD projector and a unique fringe pattern. They got different images from the studied object using the same fringe pattern for different positions of the object which was put on a rotatory table. Processing these images, it was possible to build the 3D profile and create a CAD model. This profile was used to choose the sequence measurement plain, the number and type of probe that would be used by the CMM on the object digitalization and on a second moment the final model building with a better measuring accuracy if compared to the use of just one methodology isolated.

In this work, an optical system of Fringe Projection was used to describe the 3D profile of a turbine blade. Two types of fringe pattern were used: parallel square grating pattern and parallel cosine grating pattern. For the first case, it

was chosen to use four shifted fringe patterns keeping the same fringe frequency, and on the second one four shifted fringe patterns for each different fringe frequency.

2. Methodology

The optical measurement set-up is shown in Fig. 1. It consisted of a LCD projector, with 1024 x 768 pixels resolution, placed at a distance l_p, which projected vertical fringes, i.e. in y-direction, under an oblique angle θ upon the specimen surface. A digital photographic camera, at a distance l_k, observed the fringe pattern normally to the central of the specimen surface, i.e. in z-direction. Firstly, the fringe pattern formed by a reference plane (z = 0) was observed. Then, the reference plane was replaced by the freeform surface. The two dimensional digital images (face/reference plus fringe patterns) were captured by a computer and fed into a specific software in order to retrieve the contour information using the concepts of Fringe Projection.

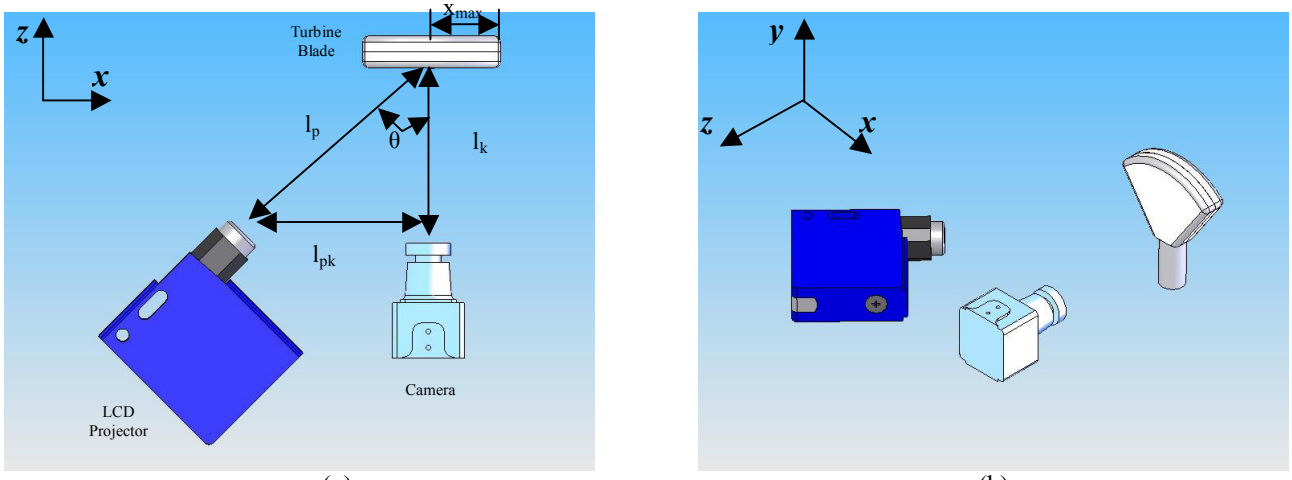

(a) (b)

Figure 1: Sketch of optic-mechanical system configuration: (a) top view and (b) isometric view.

In order to automatically quantify the surface contour, the measurement technique was combined with Phase-Shifting technique. A temporal phase shift of 270° was introduced to the grating pattern by lateral translation, such that one fringe exactly replaced its neighbouring fringe. Usually, phase shifting is introduced by lateral displacement of the grating or changing gratings in the form of slides in a slide projector. In this work, four digital grating patterns were used for illumination with a LCD projector (beamer). They were digitally displaced in x-direction by exactly ¼ of the grating pitch, introducing mutual phase steps of ninety degrees. Like that, a total of eight images were captured for each set up: four for the reference plane and four for the analysed surface.

Moreover, in this present work, two geometrical configurations illustrated at Tab. 1 and two types of fringe patterns were used. On the first, parallel square grating patterns with a number of one hundred twenty eight projected fringes were adopted. On the second, in order to improve the measurement results parallel cosine grating patterns for different fringe frequency: thirty, sixty four and one hundred projected fringes were used. All grating patterns were obtained digitally which made the phase shifting easier because it could be done by software and there was no need of using moving parts in order to improve this technique.

Table 1. Used geometric configurations.

Configuration	l_p [mm]	l_k [mm]	l_{pk} [mm]	θ [°]	x_{max} [mm]
1	1201,0±10	1040,0±10	600,0±10	-29,9±2	139±1
2	707,0±10	500,0±10	500,0±10	-45,0±2	139±1

Also, on the first methodology two main steps were adopted: phase calculation and filtering and phase unwrapping by a specific algorithm in order to remove the phase jumps. These two steps were done separately for each group of shifted images, firstly for the reference images and later on for the surface images. So, two unwrapped phase maps were obtained: one for the reference and other for the blade. Then, it was calculated the difference between them. Moreover, this difference had its sine and cosine components separated and filtered. Afterwards, the phase was rebuilt and once

more unwrapped. Finally, the fringe order of this difference was calculated and the 3D face depth map could be obtained.

The second methodology was adopted trying to improve the measurements results and reduce the computational effort. On this case, only the phase calculation was performed separately for the reference and for the blade. Then, the phase difference (reference minus blade) was evaluated. Finally, the phase unwrapping algorithm was applied and the fringe order was obtained. No filtering process was used. The same procedure was done by the three fringe frequencies. A turbine blade manufactured on cast iron with main dimensions of 139 mm x 102 mm x 35 mm, was measured in this work. Its surface was painted with a white ink in order to avoid high reflectance and improve the fringes contrast. On the first methodology one side of the turbine blade was measured and on the second methodology the opposite side was evaluated.

2.1. Depth map calculation

Considering the three dimensional configuration of Fig. 1, it was possible to write the depth map *Z* of the studied freeform surface from Eq. (1). In that equation the variables *Z* and ψ are functions of the *x* and *y* coordinates. The fringe order ψ is related to the fringe phase modulation, ϕ, and can be written as $\psi(x, y) = \phi(x, y) / 2\pi$.

$$Z(x,y) = S \cdot lp \cdot \psi(x,y)\left[\sin\theta + \frac{(l_k - l_p\cos\theta)\cdot x}{l_k \cdot l_p}\right]^{-1}\left[1 + \frac{x\cdot\sin\theta}{l_p}\right]^{2} \quad (1)$$

Where:

Z (x, y): Surface depth map;

S: Mounting sensitivity given by the ratio of the grating period with $\theta = 0$ at the specimen surface and its distance to the projection lens;

l_p: Distance between the projection unit and the centre of the studied surface;

l_k: Distance between the digital camera and the centre of the studied surface;

θ: Projection angle;

x: Parameter comprehended at interval $[-x_{max} \leq x \leq x_{max}]$ according to measured surface length;

ψ *(x, y)*: Fringe order.

Excepting the fringe order, ψ *(x, y)*, all parameters of Eq. (1) are geometrical constants defined by the optic-mechanical configuration. So, in order to calculate the depth map *Z(x, y),* the measuring system must quantify the fringe order for each image point. This can be obtained by the calculation of the phase map, ϕ *(x, y)*. However, this phase map can have phase jumps for each 2π which must be removed. Thus, phase unwrapping techniques must be applied. It is only the unwrapped phase map that will permit the corrected fringe order and, consequently, the depth map calculation, as showed by (Gäsvik, 2002).

Furthermore, Eq. (1) shows a significant non-linear dependency of contour Z with increasing *x*. Although the first dependency could be minimised by placing the projector at the same distance from the specimen surface like the camera, the second dependency, however, might not be neglected. This is true because the present system does not obey the condition of Scheimpflug, necessary to keep the projected grating pitch constant and in focus along *x*-direction. For instance, considering a projection angle, θ, of 45°, introducing errors smaller than 1% by neglecting the second dependency on *x* requires ratios between projector distance and half object length larger than 140. Such large ratios are impossible to achieve with LCD projectors and the second x-dependency in Eq. (1) is considered in the calculus of the depth map (Vecchio *et al.*, 2005).

3. Results

The following figures show the results obtained by the first methodology used. Figure 2 shows the projected images and the preliminary obtained results. Figure 2a to Fig. 2d show the studied surface and each shifted fringe pattern used. The others illustrate the phase difference (reference phase minus blade phase), the raw sine component of the phase difference, the filtered sine component and finally the unwrapping filtered phase difference map, respectively. The sine and cosine components were filtered on the frequency domain making use of a Butterworth filter of second order and cut frequencies of 50 and 150, respectively for *x* and *y* axis. The Fourier spectrum for the raw and filtered component is shown at Fig. 3.

Figure 4 shows the turbine blade two and three dimensional depth maps (2D and 3D). The measurement scales for all maps are presented in millimetres unit.

The second methodology results will be shown in sequence. Figure 5 shows the turbine blade images for each phase shifting for thirty (Fig. 5a to Fig. 5d), sixty four (Fig. 5e to Fig. 5h) and one hundred projected fringes (Fig. 5i to Fig. 5l). Figure 6 shows the resulting processed images for this adopted methodology, it illustrates, respectively, the

turbine blade phase, the reference phase, the phase difference (reference minus blade) and finally the fringe order. Figure 6a to Fig. 6d show the results for thirty projected fringes, Figure 6e to Fig. 6h illustrate the results for sixty four projected fringes and consequently Fig. 6i to Fig. 6l show the results for one hundred projected fringes.

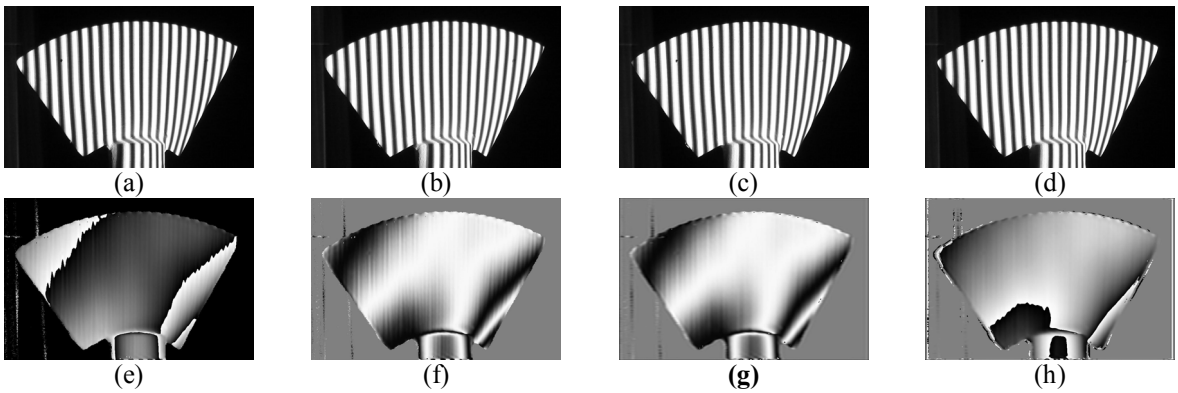

Figure 2 – Turbine blade and its four shifted fringes, **a** – 0º; **b** – 90º, **c** – 180º and **d** – 270º; **e** – phase difference, **f** – raw sine component; **g** – filtered sine component of the phase difference and **h** – filtered phase difference.

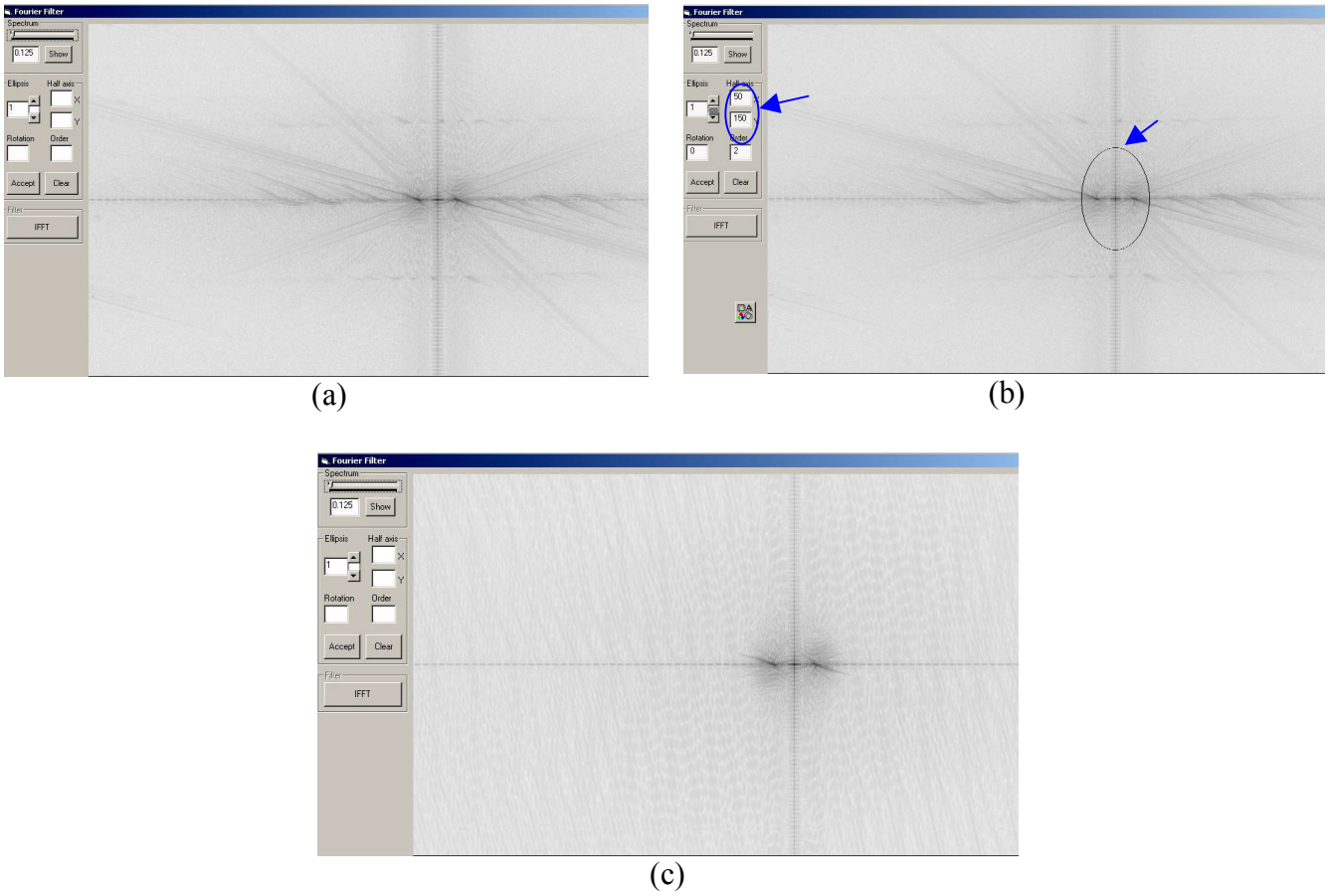

Figure 3 – Fourier spectrums, **a** – Fourier raw sine spectrum; **b** – Used cut frequencies (indicated) and **c** – Filtered sine spectrum.

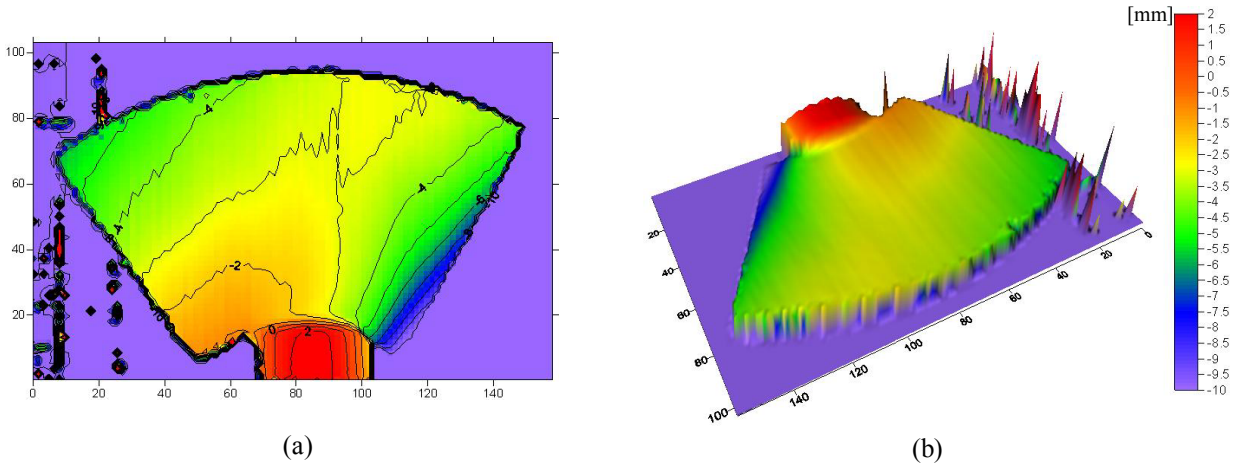

(a) (b)

Figure 4 – Calculated blade depth maps: **a –** 2D profile and **b –** 3D profile.

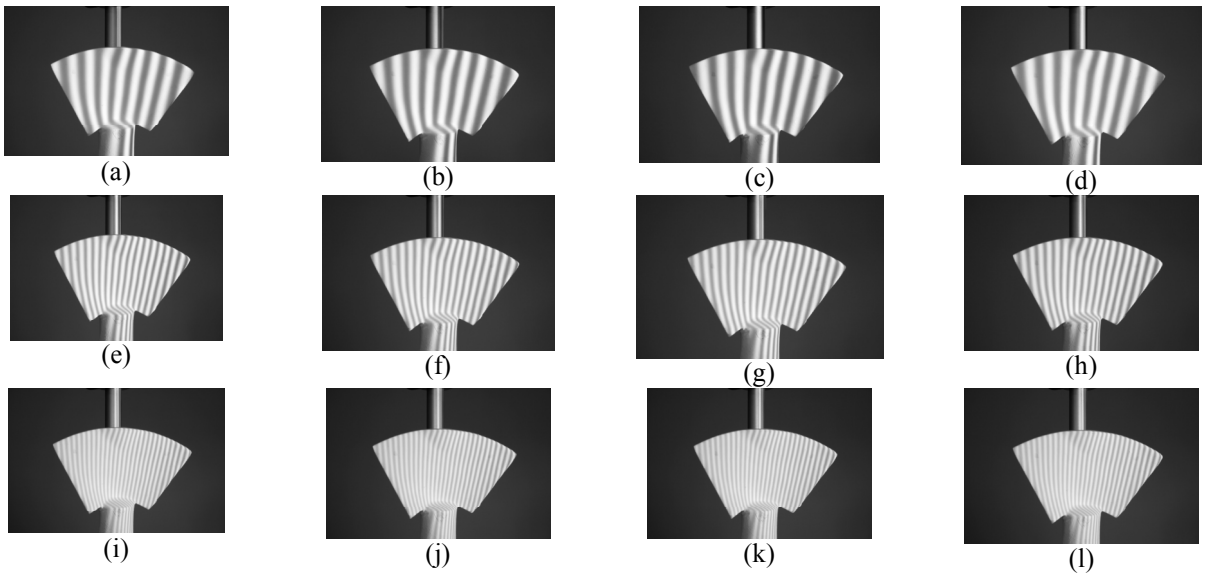

(a) (b) (c) (d)
(e) (f) (g) (h)
(i) (j) (k) (l)

Figure 5 – Turbine blade and its four shifted projected fringes for each fringe frequency, **a; e; i –** 0º; **b; f; j** – 90º, **c; g; k** – 180º and **d; h; l** – 270º.

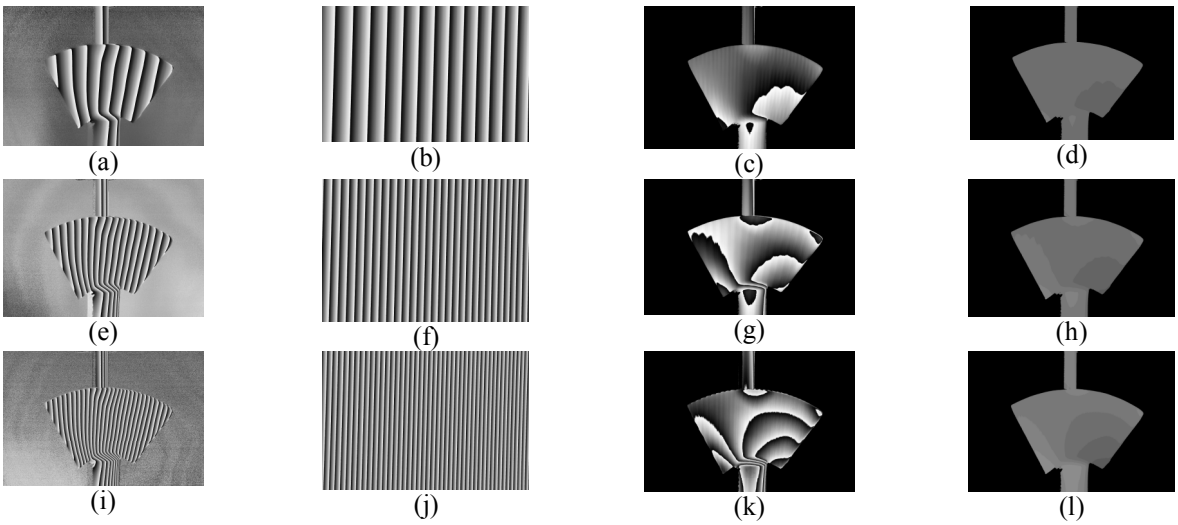

(a) (b) (c) (d)
(e) (f) (g) (h)
(i) (j) (k) (l)

Figure 6 – Intermediated results for each fringe frequency: **a; d; i** – Turbine blade phase maps; **b; e; j** –Reference phase maps; **c; f; k -** Phase differences (reference minus blade) and **d; h; l** – Fringe orders.

Figure 7 shows the turbine blade 2D depth maps calculated for each fringe order presented above. Figure 7a represent the results for thirty projected fringes, Fig. 7b shows the depth map for sixty four projected fringes and Fig. 7c shows the depth map for one hundred projected fringes.

The aim of this work was to develop an optical system able to measure freeform surfaces. So it can be seen that the processing software still has to be implemented. However, comparing the first and second methodologies it can be seen that it is reasonable reducing the computational effort during the images processing. Moreover, it can be observed that for the turbine blade analysed a higher number of projected fringes produced a better measurement result. That is true mainly if Fig. 7 is evaluated. From this figure it can be seen that the obtained depth map for one hundred projected fringes is free from noises which are presented on the other two depth maps. This reflected on the measuring results.

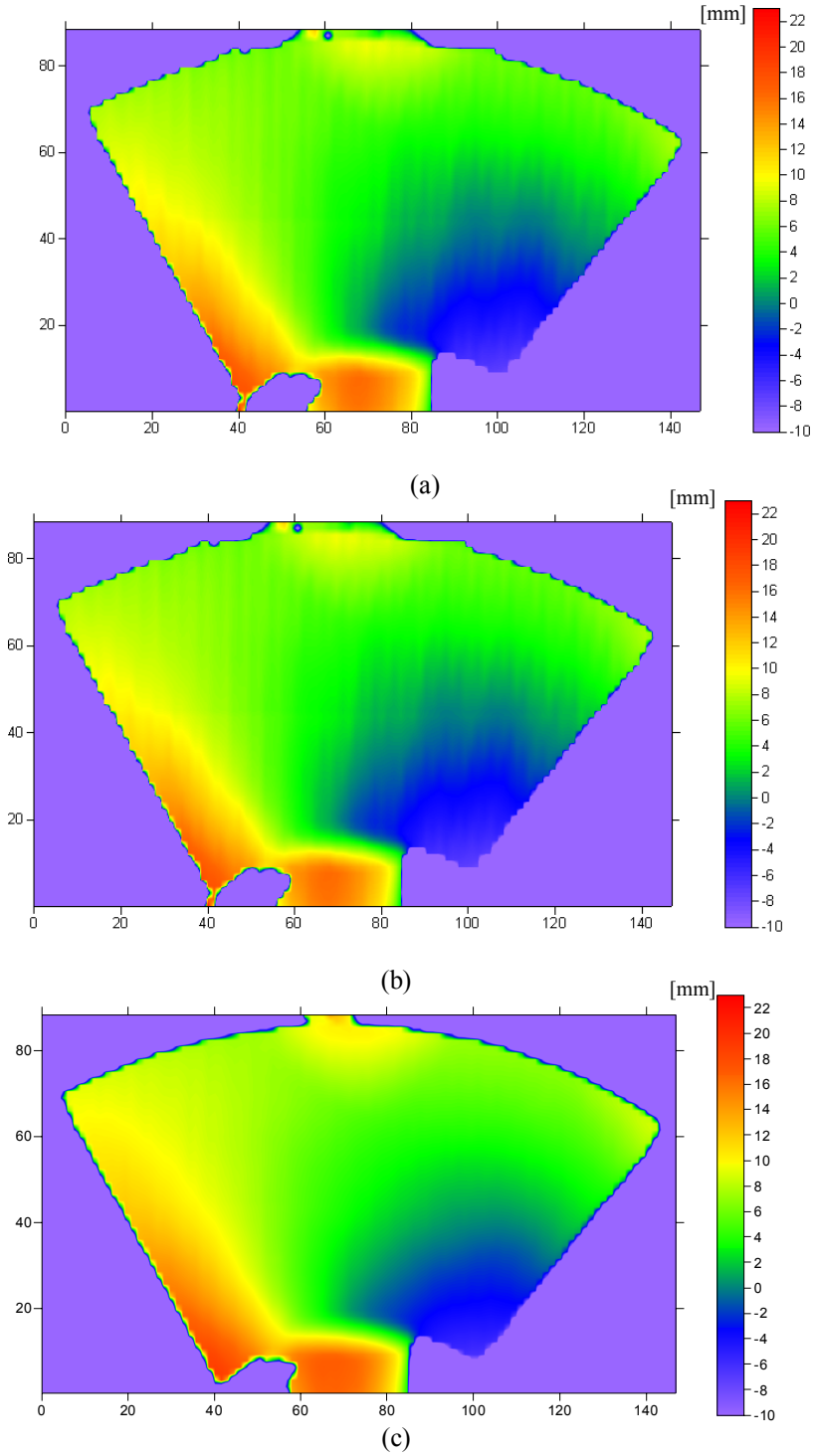

Figure 7 – Calculated turbine blade depth maps: **a** – thirty projected fringes; b – sixty four projected fringes and **c** – one hundred projected fringes.

A brief uncertainty analysis, considering a normal distribution, estimated a relative uncertainty value of 8% for the analysed blade, according to Eq. (2):

$$\frac{U_{95}(Z)}{Z}=\left\{\begin{array}{l}\left(\frac{U_{95}(s)}{s}\right)^2+\left(U_{95}(x)*A\right)^2+\left(\frac{U_{95}(\psi)}{\Psi}\right)^2+\\ +\left(U_{95}(\theta)*B\right)^2+\left(\frac{U_{95}(l_p)}{l_p}*C+\frac{U_{95}(l_k)}{l_k}*D\right)^2\end{array}\right\}^{\frac{1}{2}} \tag{2}$$

Where:

$$A=\left(\frac{l_k-l_p\cdot\cos\theta}{l_p\cdot l_k}\right)\left[sen\theta+\frac{(l_k-l_p\cdot\cos\theta)\cdot x}{l_p\cdot l_k}\right]^{-1}+\frac{2sen\theta}{l_p}\left(1+\frac{x\cdot sen\theta}{l_p}\right)^{-1} \tag{3}$$

$$B=-\left(\cos\theta+\frac{x\cdot sen\theta}{l_k}\right)\left[sen\theta+\frac{(l_k-l_p\cos\theta)\cdot x}{l_p l_k}\right]^{-1}+\frac{2x\cdot sen\theta}{l_p}\left(1+\frac{x\cdot sen\theta}{l_p}\right)^{-1} \tag{4}$$

$$C=1+\frac{x}{l_p}\cdot\left[sen\theta+\frac{(l_k-l_p\cos\theta)\cdot x}{l_p\cdot l_k}\right]^{-1}-\frac{2x\cdot sen\theta}{l_p}\cdot\left(1+\frac{x\cdot sen\theta}{l_p}\right)^{-1} \tag{5}$$

$$D=\frac{1}{l_k}\left[x\cdot\cot an\theta+l_p\cdot\cos\theta-l_k\right] \tag{6}$$

The parameter values of the above equations were presented on Tab. 1 and also are shown on Tab. 2. $U_{95}(s)/s$ represents the relative expanded sensibility uncertainty S, $U_{95}(x)$ is the uncertainty for the x parameter, $U_{95}(\theta)$ is the uncertainty for the projection angle θ, $U_{95}(l_p) / l_p$ and $U_{95}(l_k) / l_k$ represent, respectively, the relative uncertainty for distances l_p and l_k.. The value for the relative phase uncertainty, $U_{95}(\psi)/\psi$, was chosen according to (Yatagai, 1993). The other values correspond to the measuring systems uncertainties used on the set up of the system (Vecchio, 2006).

Table 2. Adopted uncertainty values

$U_{95}(s)/s$	0,010
$U_{95}(x)$	1,000 mm
$U_{95}(\psi)/\psi$	0,050
$U_{95}(\theta)$	0,035 rad
$U_{95}(l_p)/l_p$	0,010
$U_{95}(l_k)/l_k$	0,010

It could be noted that the most relevant uncertainty contributions were the phase uncertainty and the projection angle. This demonstrates that the measurement uncertainty depends greatly from how better phase measurements are processed and also from geometrical system configuration, as it was already commented by (Quan *et a*l., 1999). However, software and experimental implementations have been still in process to improve the final results. This will contribute for the accuracy of the measurement results.

4. Conclusion

The results show that the reduction on the computational effort did not interfere on the final measurements. Also, the use of high fringe frequencies is reasonable for surfaces which have soft geometries. Other relevant point to consider overlays the fact that it is possible to calculate the phase difference between the reference and surface through wrapped phase maps. In addition, different from the first methodology, on which the phases for the turbine blade, for the reference and also for the difference were filtered on the frequency domain, no filtering step was used on the second methodology, reaching, however, the same results. The results can be still implemented by using a filter, which can improve the final results. Also, the use of cosine grating patterns instead of square types seems to produce better results mainly because Eq. (1) was mathematically concept through sine functions. So, the physical phenomenon was better

modelled. On a future work, it can be made the complete rebuilding of the turbine blade combining the measurement results for both sides of it as already described by (Carbone et al., 2001).

Furthermore, it could be seen that the greatest advantage of Fringe Projection technique is the simplicity, absence of moving parts and low cost compared to other digital measuring systems. Moreover, the object length is not a prohibited factor and it can be placed in any position, i.e., vertical or horizontal. It is a non-contact measurement technique which permits the geometric control of surfaces showing its powerful application on industrial inspection.

5. References

Carbone, V., Carocci, M; Savio, E. Chiffre, L. De., 2001, "Combination of a vision system and a coordinate measuring machine for the reverse engineering of freeform surfaces." *International Journal of Advanced Manufacturing Technology*, v. 17, p. 263-271.

Durelli, A.J., Parks, V.J., 1970, *Moiré Analysis of Strain*. Prentice-Hall, Englewood Cliffs, NJ, 1970.

Gäsvik, K. J., 2002, *Optical metrology*. 3. ed. England: John Wiley & Sons Ltd, 360 p.

Gäsvik, K.J.; Hovde, T.; Vadseth, T., 1989, "Moiré technique in 3D machine vision". *Optics and Lasers in Engineering*, v. 10, p. 241-249.

Lu, C.; Yamaguchi, A.; Inokuchi, S., 2002, "3D measurement based on intensityphase analysis of intensity modulated Moiré." *Electronics and Communications in Japan*, part 3, v. 85, n. 1, p. 71-80.

Meadows, D. M., W. O. Johnson, and J. B. Allen, 1970, "Generation of Surface Contours by Moiré Patterns," Appl. Opt., 9(4), 942-947 (1970).

Post, D.; Han, B.; Ifju, P., 1994, "*High sensitivity moiré*: experimental analysis for mechanics and materials." 1. ed. Springer-Verlag New York; 444 p.

Quan, C.; Tay, C. J.; Shang, H., M., 1999, "Fringe projection technique for the 3D shape measurement of a hydroformed shell." *Journal of Materials Processing Technology,* v. 89, n. 90, p. 88-91.

Takasaki, H., 1970, "Moire Topography," Appl. Opt., v.9, n. 6, p.1467-1472.

Theocaris, P., 1969, *Moiré Fringes in Strain Analysis*, Pergamon Press, London.

Vecchio, S.D.; Campos, I.L.P.; Sesselmann, M.; Pinotti, M., 2005, "*Study of projection Moiré technique applied to free contour measurements in bioengineering."* In: 18th International Congress of Mechanical Engineering, 2005, Ouro Preto - MG. Proceedings of the 18th International Congress of Mechanical Engineering. Rio de Janeiro - RJ: Associação Brasileira de Engenharia e Ciências Mecânicas - ABCM. v. 1. p. 1-8.

Vecchio, Sara Del., 2006, "*Medição de superfícies livres tridimensionais a partir da técnica de Moiré de projeção."* 2006. 125 f. Dissertação (Mestrado em Engenharia Mecânica) – Departamento de Engenharia Mecânica, Escola de Engenharia, Universidade Federal de Minas Gerais, Belo Horizonte.

Yatagai, T., 1993, "Interferogram Analysis: Intensity based analysis methods", avaiable at chapter 3, Ed. David W. Robinson & Graeme T. Reid, 302 p.

Yoshizawa, T.; Otani, Y., 1989, "Moiré topography with submicron sensitivity." *Precision Engineering*, v. 55, p. 152-154.